# Charge and spin state of dilute Fe in NaCl and LiF

H. P. Gunnlaugsson,[1] A. Mokhles Gerami,[2,3] H. Masenda,[4] S. Olafsson,[1] R. Adhikari,[5] K. Johnston,[3] K. Naicker,[6] G. Peters,[4] J. Schell,[3,7] D. Zyabkin,[8] K. Bharuth-Ram,[6] P. Krastev,[9] R. Mantovan,[10] D. Naidoo,[4] I. Unzueta,[11] and ISOLDE Collaboration[3]

[1]*University of Iceland, Dunhaga 3, IS-107 Reykjavík, Iceland*

[2]*School of Particles and Accelerators, Institute for Research in Fundamental Sciences (IPM), P.O. Box 19395-5531, Tehran, Iran*

[3]*European Organization for Nuclear Research (CERN), CH-1211 Geneva, Switzerland*

[4]*School of Physics, University of the Witwatersrand, Johannesburg 2050, South Africa*

[5]*Institute for Semiconductor and Solid State Physics, Johannes Kepler University, Altenbergerstr. 69, Linz, Austria*

[6]*School of Chemistry and Physics, University of KwaZulu-Natal, Durban 4001, South Africa*

[7]*Institute for Materials Science and Center for Nanointegration Duisburg-Essen (CENIDE), University of Duisburg-Essen, 45141 Essen, Germany*

[8]*Chair Materials for Electrical Engineering and Electronics, Institute of Materials Science and Engineering, Institute of Micro and Nanotechnologies MacroNano®, TU Ilmenau, Gustav-Kirchhoff-Strasse 5, 98693 Ilmenau, Germany*

[9]*Institute for Nuclear Research and Nuclear Energy, Bulgarian Academy of Sciences, 72 Tsarigradsko Chaussee Boulevard, Sofia, 1784, Bulgaria*

[10]*CNR-IMM Unit of Agrate Brianza, Via Olivetti 2, I-20864 Agrate Brianza (MB), Italy*

[11]*Department of Applied Physics, School of Engineering Gipuzkoa, University of the Basque Country (UPV/EHU), Plaza Europa 1, 20018 San Sebastian, Spain*

(Received 20 March 2021; revised 10 October 2022; accepted 17 October 2022; published 16 November 2022)

There is an apparent mismatch between electron paramagnetic resonance and Mössbauer spectroscopy results on the charge and spin states of dilute Fe impurities in NaCl; Mössbauer spectroscopy data have been interpreted in terms of high-spin $Fe^{2+}$, while electron paramagnetic resonance studies suggest low-spin $Fe^{1+}$. In the present study, the charge and spin states of dilute substitutional Fe impurities in NaCl and LiF have been investigated with $^{57}Mn \rightarrow {}^{57}Fe$ emission Mössbauer spectroscopy. A scheme is proposed which takes into account the effects of nearest-neighbor distances and electronegativity difference of the host atoms on the Mössbauer isomer shift and allows for the unequivocal differentiation between high-spin $Fe^{2+}$ and high/low-spin $Fe^{1+}$ in Mössbauer spectroscopy. From these considerations, the Mössbauer results are found to be consistent with dilute Fe impurities in NaCl and LiF in a low-spin $Fe^{1+}$ state. These conclusions are supported by theoretical calculations of isomer shifts and formation energies based on the density-functional theory. The experimental results furthermore suggest that charge compensation of dilute $Mn^{2+}$ dopants in NaCl and LiF is achieved by Na vacancies and $F^-$ interstitials, respectively.

DOI: 10.1103/PhysRevB.106.174108

## I. INTRODUCTION

In order to estimate the charge and spin state of Fe in materials, one suggested approach is to compare the Mössbauer isomer shift, $\delta_{RT}$, to experimentally determined ranges of Mössbauer isomer shifts of known charge/spin states [1]. Although the measured isomer shift ranges overlap considerably, high-spin $Fe^{2+}$ is uniquely determined from the isomer shift at room temperature relative to Fe metal to be in the range $\delta_{RT} = 0.8$–$1.5$ mm/s.

Several Mössbauer studies of dilute iron impurities in NaCl exist [2–8]; two authors report single-line spectral components as expected for substitutional Fe in cubic symmetry. Kai [7] observed a single line in $^{57}Fe$ doped NaCl with an isomer shift of $\delta_{RT} = 1.15(1)$ mm/s and attributed this line to $Fe^{2+}$ on substitutional Na site with an unknown charge-compensating defect nearby. Barb *et al.* [8] also observed in $^{57}Fe$-doped NaCl a single line with an isomer shift of $\delta_{RT} = 1.13$ mm/s which the authors attributed to a stable mixture of high-spin $Fe^{2+}$ and Na vacancies in the NaCl structure in the Suzuki phase [9]. In both of these studies the single lines were ascribed to high-spin $Fe^{2+}$, as is expected from comparison of the experimental isomer shift with ranges of isomer shifts of known charge/spin states [1].

Results in some earlier papers (see, e.g., Refs. [2–6] and references therein) differ significantly. In all cases, spectral components that could be interpreted as due to high-spin $Fe^{3+}$ doublets are reported. This suggests that Fe is not dilute in the

samples, as dilute $Fe^{3+}$ (<0.1 at. %) would be expected to show slow paramagnetic relaxations with characteristic magnetic hyperfine field split components [10]. Mullen [2] and Edelglass and Ohring [5] reported a single line with an isomer shift $\delta_{RT} \sim 2$ mm/s which was attributed to $Fe^{1+}$. Based on their experimental data, however, this line could be interpreted as due to one peak of a quadrupole split high-spin $Fe^{2+}$ component, with the other peak overlapping with the dominating $Fe^{3+}$ doublet component.

Electron paramagnetic resonance (EPR) studies on dilute iron impurities in NaCl [11,12] and LiF [13] suggest low-spin $Fe^{1+}$in these two systems.

In NaCl, the EPR data showed after irradiation association of the low-spin $Fe^{1+}$ with a vacancy on the Na site ($V_{Na}$) which was stable up to ~200 K. Above this temperature, the vacancy was found to move away and an unperturbed cubic $Fe^{1+}$ formed. It should be noted that EPR may not be sensitive to high-spin $Fe^{2+}$ due to the integer spin. Therefore, it is unclear whether high-spin $Fe^{2+}$ could still be the dominating Fe species in NaCl, in accordance with conclusions from Mössbauer studies.

Mössbauer spectroscopy experiments of Fe impurities in LiF [6,14] did not reveal any single-line spectral components that could be attributed to Fe on substitutional sites but rather quadrupole-split components that could be ascribed to a mixture of high-spin $Fe^{3+}$ and $Fe^{2+}$.

In this paper, we report our investigation of the apparent discrepancy in the determination of the natural spin/charge state of dilute Fe in NaCl by Mössbauer spectroscopy (MS) and electron paramagnetic resonance with emission Mössbauer spectroscopy (eMS) data and complementary first-principle calculations using the density-functional theory (DFT).

## II. EXPERIMENT AND THEORETICAL DETAILS

Beams of $^{57}$Mn ($T_{1/2} = 1.45$ min.) ions were produced at the ISOLDE radioactive ion-beam facility at European Organization for Nuclear Research (CERN) by 1.4-GeV proton-induced fission in a heated $UC_x$ target, Mn laser ionization [15], and acceleration to 50 keV. The $^{57}$Mn ions were implanted into commercially acquired NaCl and LiF crystal samples (Crystran) heated from behind with a halogen lamp. A maximum of $10^{12}$ $^{57}$Mn /cm$^2$ were implanted in each sample, corresponding to local concentration $<4 \times 10^{-4}$ at. %. Implantations took place at 30° relative to the sample surface normal. eMS spectra were measured on the $^{57}$Fe 14.4-keV Mössbauer radiation, at 60° emission angle relative to the sample surface normal, with a parallel-plate avalanche detector [16] equipped with stainless-steel electrodes enriched in $^{57}$Fe. Isomer shifts and velocities are given relative to the Mössbauer spectrum of $^{57}$Fe in $\alpha$-Fe at room temperature (RT). The intrinsic linewidth of the system was simulated with a Voigt line shape with Lorentzian broadening of 0.34 mm/s and Gaussian broadening of 0.10 mm/s. All spectra were analyzed using the analysis code VINDA [17].

NaCl and LiF are both of rocksalt structure, with lattice constants 5.644 02 and 4.0351 Å, respectively. Both compounds give rise to ionic bindings with a difference in (Pauling) electronegativity of $\Delta\chi_P = 2.23$ for NaCl and $\Delta\chi_P = 3.0$ for LiF.

For interpretation of the experimental results, the hyperfine parameters were obtained using first-principle calculations based on the density-functional theory [18] method which is implemented in the framework of WIEN2K [19]. All calculations for the system of NaCl and LiF were performed with the flavors of generalized gradient approximations of Perdew-Burke-Ernzerhof before (PBE) [20].

As an all-electron method, WIEN2K has been proven to be a benchmark to compute hyperfine parameters. In the present calculations the hyperfine parameters of Fe replacing Na or Li in NaCl and LiF, respectively, have been calculated and the case of low- and high-spin state have been considered for the $d$-orbital band of the Fe atom. The Fe, Na, and Cl radii (in Bohr radii, $a_0$) of the muffin-tin atomic spheres were, respectively, set to 2.5, 2.3, and 2.2 $a_0$ in the Fe-doped NaCl lattice, and the corresponding values of the Fe, Li, and F radii set to 1.95, 1.60, and 1.82 $a_0$, respectively, for the Fe-doped LiF system. The energy boundary between core and valence electronic states was −6 Ry, the cutoff parameter $R_{MT} \times K_{max}$ (which controls the size of the basis set) was 7.0 $(a_0)^{-1}$, and $G_{max}$, the Fourier expansion of the charge density, was restricted to 16 $(Ry)^{1/2}$. In order to compare the calculated hyperfine parameters with experimental results, the simulations were performed using supercell size of $2 \times 2 \times 2$ unit cells, corresponding to a nominal Fe concentration of 3.12%. The experimental lattice constant and atom position data at room temperature are taken from Ref. [21] for NaCl and from Ref. [22] for LiF. The internal atomic positions are minimized to a force limit below 1 mRy/Å. A mesh of $(6 \times 6 \times 6)$ $k$ points in the irreducible part of the first Brillouin zone was applied to the self-consistent total energy calculation. All calculations are done considering spin-polarized states for both high-spin and low-spin states which give magnetic moment and a measure of spin alignment. The method to fix the total magnetic moment of the system [18] when initiating calculations was applied for low-spin cases.

The isomer shift is obtained from the contact densities ($\rho$) [23] as $\delta = \alpha(\rho_A - \rho_S)$, where $\rho_A$ and $\rho_S$ are the charge densities at the probe nucleus in the absorber ($A$) and sample ($S$) material, respectively. The calibration constant of $\alpha = -0.29$ $a_0^3$. mm/s, as in Ref. [24], was used. The electric-field gradient tensor, expressed by its principal component ($V_{ZZ}$) and the asymmetry parameter ($\eta$), gives the quadrupole splitting as $\Delta E_Q = \frac{eQV_{ZZ}}{2}\sqrt{1+\eta^2/3}$ [25], where $e$ is the elementary charge and $Q = 0.16 \times 10^{-28}$ m$^2$ is the nuclear quadrupole moment of the 14.4 keV Mössbauer state of $^{57}$Fe.

## III. RESULTS AND ANALYSIS

### A. NaCl

Details of the Mössbauer spectrum obtained at RT following the Mn/Fe implantation in the NaCl single-crystal sample are highlighted in Fig. 1, where six clear features are identified and labeled, from No. 1 to No. 6. Figure 2 shows the final analysis of temperature-dependent data measured in the range 300–626 K.

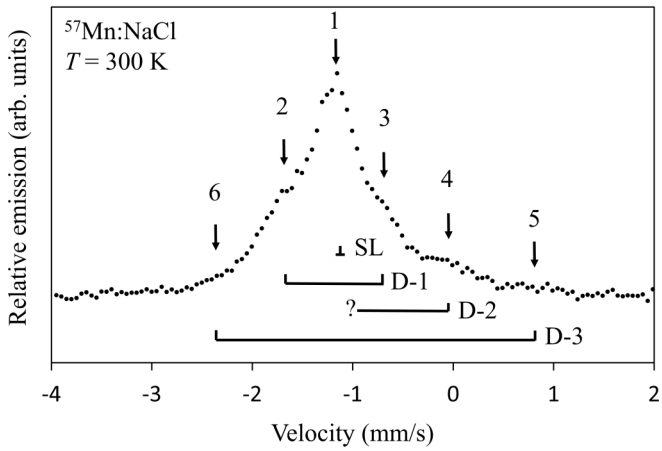


FIG. 1. Details of the $^{57}$Fe eMS spectrum obtained after implantation of $^{57}$Mn into a NaCl sample at room temperature. Numbers indicate spectral features and their relation to spectral components (SL, D-) discussed in the text.

The dominant central feature (No. 1 in Fig. 1) is observed throughout the temperature series and is assigned to a single-line (SL) spectral component. The features on the shoulder of the SL (No. 2 and No. 3 in Fig. 1) observed at RT merge into the SL at elevated temperatures (cf. Fig. 2), indicating a component with temperature-dependent quadrupole splitting (D1). A feature observed at velocity $v \sim 0$ mm/s (No. 4 in Fig. 1) intensifies at elevated temperatures. Its position does not follow the expected second-order Doppler shift with increasing temperature but moves more towards the left in the spectrum. This indicates that this line feature corresponds to the right peak of a quadrupole-split component (D2) where the left peak overlaps the dominating features No. 1–No. 3 in Fig. 1. Finally, there are small features (No. 5 and No. 6 in Fig. 1) whose intensities increase with temperature, supporting their assignment to two peaks of a quadrupole-split component (D3) with large splitting at room temperature.

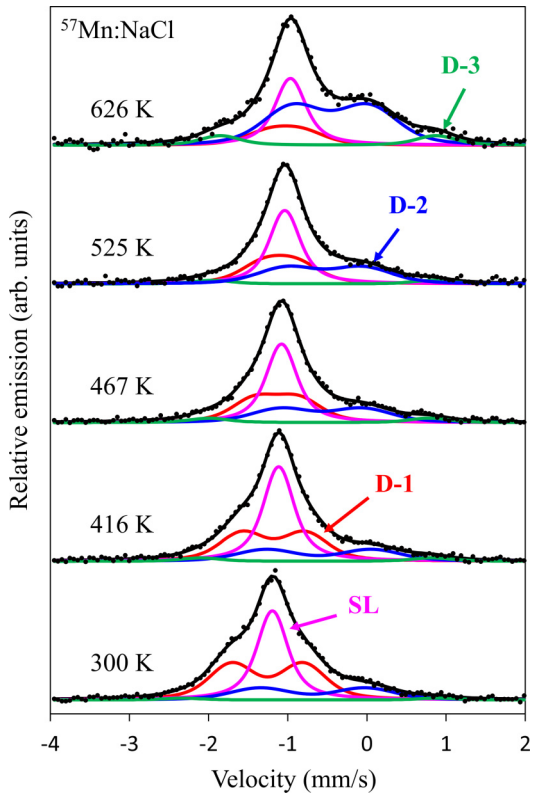


FIG. 2. $^{57}$Fe eMS spectra obtained after implantation of $^{57}$Mn into NaCl crystals held at the temperatures indicated. Solid lines show the fitting components and their sum.

TABLE I. Hyperfine parameters obtained from the analysis of the eMS spectra in NaCl (Fig. 2). Table lists the isomer shift ($\delta_{RT}$) and quadrupole splitting ($\Delta E_{Q,\,RT}$) at room temperature, additional Gaussian linewidth broadening ($\Delta\sigma$) taking into account the linewidth of the detector, and a site assignment substantiated in the text. The numbers in the parentheses represent the error in the last digit, calculated assuming pairwise-coupled variables.

| Component | $\delta_{RT}$ (mm/s) | $\Delta E_{Q,RT}$ (mm/s) | $\Delta\sigma$ (mm/s) | Site assignment |
|---|---|---|---|---|
| SL | 1.19(2) | | 0.00(3) | $Fe_{Na}^{1+}$ |
| D1 | 1.26(3) | 0.90(5) | 0.10(3) | $Fe_{Na}^{1+} - V_{Na}$ |
| D2 | 0.69(10) | 1.33(6) | 0.19(7) | $Fe_{Na}^{2+} - Cl_I$ |
| D3 | 0.72(6) | 3.2(4) | 0.07(10) | Unknown |

The final analysis of the spectra collected in the temperature series was done simultaneously in terms of the components outlined above, where the positions of components were restricted to follow the expected second-order Doppler shift with temperature and linewidths restricted to have a temperature-independent Gaussian broadening. The resulting Mössbauer spectra obtained after implantation into NaCl at the temperatures indicated, together with the fitted components, are shown in Fig. 2.

The analysis model applied here sufficiently describes the experimental data, the greatest inaccuracy being with the quadrupole-split component D2 due to its left peak being obscured under the central peaks. The temperature dependence of the total area follows the Debye approximation with a Debye temperature $\theta_D \sim 200$ K, in good agreement with mass defect approximation of Debye-Waller factors determined from compressibility data [26]. There is no evidence of a spectral component with low Debye temperature that could be interpreted as being due to interstitial Fe. The hyperfine parameters extracted at room temperature are gathered in Table I. The temperature dependence of the quadrupole splitting of the doublet components is shown in Fig. 3.

Fe substituting for octahedrally coordinated $Na^+$ in defect-free NaCl would be expected to be observed as a single line; only the SL component is consistent with this property. The isomer shift of this line, $\delta_{RT} = 1.19(2)$ mm/s, is in reasonable agreement with the isomer shift determined by Refs. [7,8] and falls in the center of the range expected for high-spin $Fe^{2+}$ but far from the range $\delta_{RT} = 0.2$–$0.3$ mm/s expected for low-spin $Fe^{1+}$ [1].

The above considerations may lead one to conclude that the dilute Fe in NaCl is in high-spin $Fe^{2+}$ state with a nearby charge-compensating defect. There are, however, problems

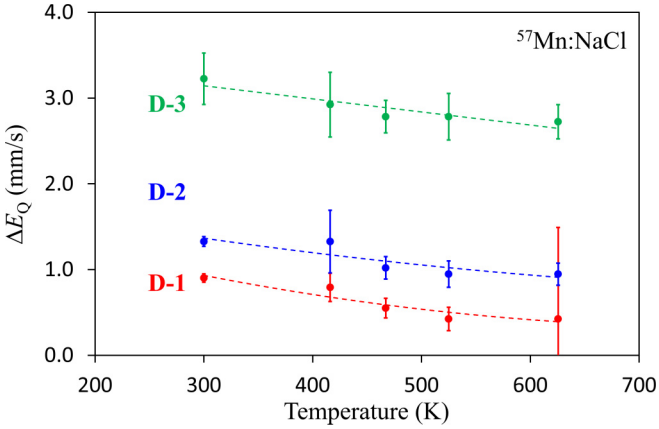


FIG. 3. Temperature dependence of the quadrupole splitting of the D1 to D3 components obtained from the analysis of the spectra shown in Fig. 2. Dashed lines are to guide the eye.

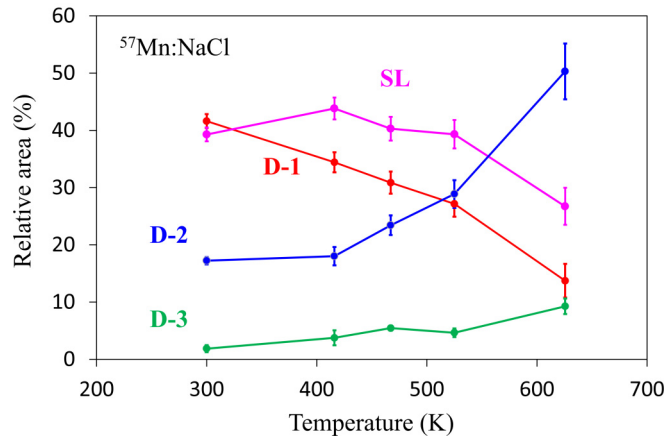


FIG. 4. Temperature dependence of the relative areas of the spectral components used to analyze the spectra (cf. Fig. 2) obtained in NaCl.

with this interpretation. The obvious candidates for charge compensation would be Na vacancy ($V_{Na}$) or $Cl^-$ interstitial ($Cl_I$). Both Yang *et al.* [11] and Nistor *et al.* [12] reported $Fe^{1+}$ associated with cation vacancy ($V_{Na}$) as nearest neighbor (nn) or next-nearest neighbors (nnn) to the low-spin $Fe^{1+}$ ion on $Na^+$ site, thus demonstrating that the $V_{Na}$ cannot be the charge-compensating defect giving Fe the 2+ charge state. $Cl_I$ at the center of the cube, in a point-charge model, would be expected to give rise to a quadrupole splitting of ∼0.45 mm/s. However, negligible splitting/broadening of the SL is observed (cf. the $\Delta\sigma$ value of SL in Table I).

This stimulated our search for an alternative explanation for the SL component other than due to high-spin $Fe^{2+}$. One explanation is that the isomer-shift ranges in Ref. [1] are not appropriate for Fe in NaCl as the effect on the isomer shift of nearest-neighbor distances and difference in electronegativity of the host are not considered. An alternative approach to account for these properties is to apply the empirical model from Ref. [27] for substitutional highs-pin $Fe^{2+}$. This model gives an isomer shift of $\delta_{RT} = 2.03(9)$ mm/s, which is ∼1 mm/s greater than the center of the range of expected isomer shifts [1] for high-spin $Fe^{2+}$. This would imply that the isomer-shift ranges in Ref. [1] are underestimated by ∼1 mm/s for substitutional impurities in NaCl as nearest-neighbor distances and difference in electronegativity of the host are not factored in. Adjusting the isomer-shift ranges in Ref. [1] by 1 mm/s, the expected range of low-spin $Fe^{1+}$ would be centered around $\delta_{RT} = 1.25$ mm/s. This matches the observed value for the isomer shift of the SL of $\delta_{RT} = 1.19(2)$ mm/s and allows us to assign component SL to low-spin $Fe^{1+}$.

The spectral component D-1 has an isomer shift slightly higher than that of the SL. Based on the observation, by EPR, of low-spin $Fe^{1+}$ associated with a sodium vacancy [11,12], it is tempting to assign D1 to the same type of defect or $Fe^{1+}_{Na} - V_{Na}$. Gunnlaugsson and Masenda [27] found that the isomer shift increases with increasing nearest-neighbor distances for high-spin $Fe^{2+}$. The same behavior is expected for low-spin $Fe^{1+}$. Removal of an atom in the vicinity of the probe atom would be expected to give rise to an increase in the nearest-neighbor distances due to the average lengthening of crystal bonds, thereby decreasing the charge density in the vicinity of the Fe probe with a consequent increase of the isomer shift. This is consistent with the observed higher isomer shift of D-1 relative to SL. The temperature-dependent quadrupole splitting then originates from temperature-dependent population of individual $e_g$ orbitals in the orthorhombic crystal field.

The area fraction of the D2 and D3 components increases significantly with increasing temperature (cf. Fig. 4). The broadening of the D2 component [$\Delta\sigma = 0.19(7)$ mm/s, Table I] suggests a distribution of local environments, which is atypical of a single type of defect structure. In order to test the hypothesis of whether D2 is due to pairing with a highly mobile defect, the area ratios of the components with implantation fluence were investigated in the spectra collected at 626 and 525 K. (cf. Fig. 5).

The relative area increases with increasing fluence from 38(3)% to 59(5)% in the measurements presented in Fig. 5. Similar results were observed in the measurements at 525 K (not shown), although the transformation at 626 K is roughly 1.8× faster than at 525 K.

The above result suggests that the D-2 component is formed as a consequence of pairing of the probe $^{57}$Mn with defects created in the implantation process, which are not mobile enough to cause paring at ∼300 K but mobile enough to cause pairing at $T > 500$ K. The isomer shift and temperature dependence of the quadrupole splitting indicate high-spin $Fe^{2+}$ species, although low-spin $Fe^{3+}$ cannot be excluded. The obvious defect candidate for increasing the charge state of the Fe atom would be interstitial $Cl^-$ leading to the tentative assignment of D2 as due to $Fe^{2+}$–$Cl^-$ pairs. Coupling to Na di-vacancies can be excluded due to the slow diffusion of the Na vacancy at these temperatures [28]. The large quadrupole splitting and isomer shift of D3 suggest that this component is due to high-spin $Fe^{2+}$. However, the intensity of this feature is too low to make any conclusions of its nature at this stage.

### B. LiF

$^{57}$Fe eMS spectra obtained after implantation of $^{57}$Mn into LiF at RT (a) and 539 K (b) are shown in Fig. 6, for which the analysis proved to be fairly complicated. A physically

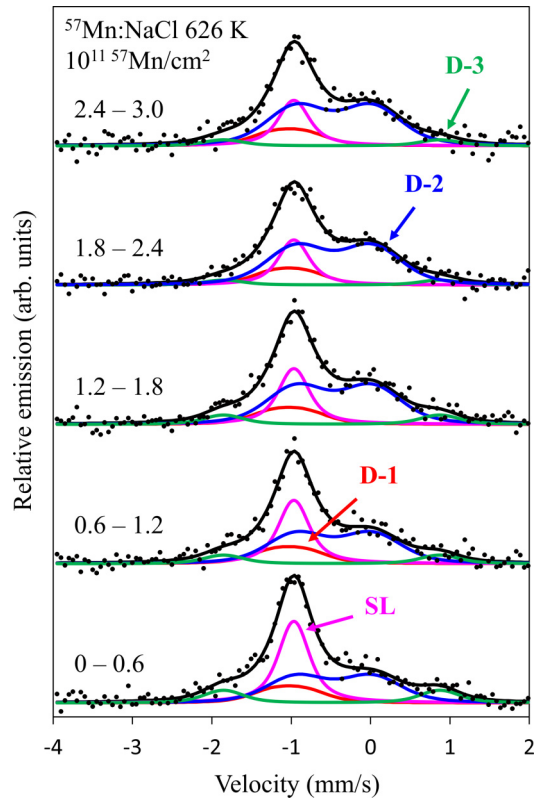


FIG. 5. Series of $^{57}$Fe Mössbauer spectra obtained after implantation of $^{57}$Mn in NaCl at 626 K for $^{57}$Mn fluences indicated, analyzed in terms of the same components as used in Fig. 2.

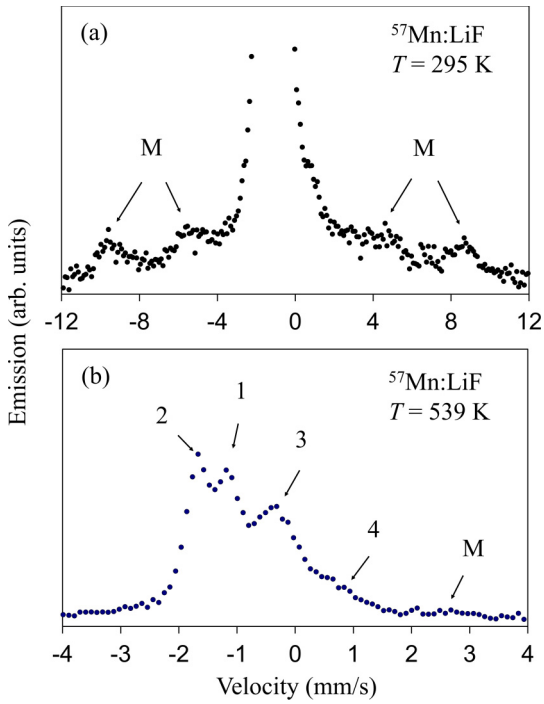


FIG. 6. $^{57}$Fe eMS spectra obtained after implantation of $^{57}$Mn into LiF at room temperature (a) and 539 K (b). Numbers and letters indicate features discussed in the text.

consistent analysis was only obtained in an iterative process described below.

At RT, the wings of the spectrum show typical signs of magnetic hyperfine field splitting [marked M in Fig. 6(a)] extending over the velocity range of ±10 mm/s. These features are found to broaden at increasing temperatures which is typical for dilute high-spin $Fe^{3+}$ showing paramagnetic relaxations times comparable with the 140-ns lifetime of the Mössbauer state [29,30]. These features were analyzed using the EmpBT model described in Refs. [29,30] with the restriction that the spin-lattice relaxation rate follows a $T^2$ temperature dependence.

The central region of the spectrum obtained at 539 K [cf. Fig. 6(b)] shows several features labeled No. 1 to No. 4. Feature No. 1 is consistent with a single line with $\delta_{RT} \sim 1.3$ mm/s. The two features No. 2 and No. 3 vary alike in intensity with temperature, which tentatively identifies these peaks as due to an asymmetrically broadened quadrupole-split component (D-1) with isomer shift very similar to that of the SL. The position of feature No. 4 does not follow the second-order Doppler shift, but moves further to the left in the spectra with increasing temperature, suggesting that it is the right leg of a quadrupole-split spectral component, with the left leg underneath the other dominant central features.

The analysis obtained with the above ansatz did not result in a physically correct picture. The left leg of D1 was found to have negligible broadening [$\Delta\sigma = 0.00(2)$ mm/s], while the right leg was significantly broadened [$\Delta\sigma = 0.19(3)$ mm/s]. This is unlikely to be due to the random distribution of environments (both peaks should be broadened), but rather due to a finite number of similar Fe sites, with negative coupling between the isomer shift and quadrupole splitting. Simple testing revealed that two symmetric spectral components replacing D1 were sufficient to describe the data. As a more physically correct model to describe the data is required, more details on D1 are needed.

The quadrupole splitting of D1 shows negligible temperature dependence, suggesting a local environment with large splitting between filled and empty orbital levels. The obvious local environment would be low-spin ($S = 0$) $Fe^{2+}$ with the $t_{2g}$ levels filled in octahedral symmetry.

At first glance, it would be attractive to assign D1 in LiF to an $Fe^{1+}$–$V_{Li}$ defect, similar to that found for D1 in NaCl, owing to the similarity in isomer shifts of SL and D1. However, such an assignment would be inconsistent with the vanishing temperature dependence of the quadrupole splitting of D1.

The obvious acceptor defects that promote the $Fe^{2+}$ state over $Fe^{1+}$ would be interstitial $F^-$ ($F_I$) or vacancy at Li site ($V_{Li}$). For low-spin $Fe^{2+}$, only noncubic arrangement of lattice atoms contributes to the quadrupole splitting. In a point-charge model, an interstitial $F^-$ ion at the center of the cube in LiF ($Fe^{2+}$–$F_I$) would result in a quadrupole splitting of $\Delta E_Q = 1.24$ mm/s, similar to the observed average quadrupole splitting 1.34(2) mm/s of D1. A similar point-charge model calculation of the effect of $V_{Li}$ results in a quadrupole splitting of 0.28 mm/s and, therefore, $F^-$ at the center of the cube is considered the more likely candidate for explaining D1 despite the crudeness of the point-charge model where structural relaxations are not employed.

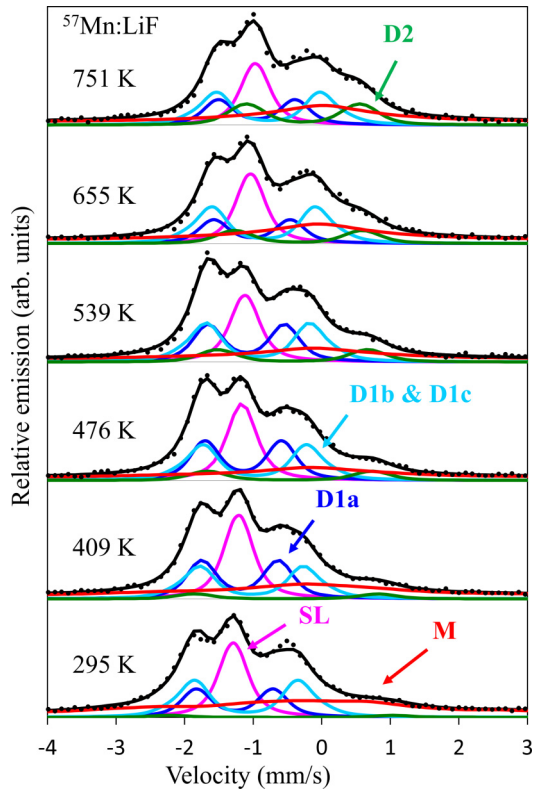


FIG. 7. Central part of the $^{57}$Fe eMS spectra obtained after implantation of $^{57}$Mn into LiF crystal held at the temperatures indicated. Solid lines show the fitting components and their sum. Shape of the *M* component within the narrow velocity range is dictated by the shape of the outer features beyond the narrow velocity range.

The consideration above does not explain the asymmetry of the D1 component. One hypothesis could be that this is due to a defect with two interstitial $F^-$. With eight possible cubic cages for the interstitial $F^-$, two interstitial $F^-$ can be constructed in seven different ways. In a point-charge model, six combinations ($Fe^{2+}$–$2F_I$) give rise to a quadrupole splitting of $\Delta E_Q = 1.43$ mm/s, while one combination ($F_I$ at opposite sides of the $Fe^{2+}$ atom or $F_I$–$Fe^{2+}$–$F_I$) gives rise to a quadrupole splitting of $\Delta E_Q = 2.47$ mm/s (twice that of $Fe^{2+}$–$F_I$).

In the final analysis, instead of a single-component D1, the spectra were analyzed with three components: D1a, assigned to $Fe^{2+}$–$F_I$ defects, D1b assigned to $Fe^{2+}$–$2F_I$ defects, and D1c assigned to $F_I$–$Fe^{2+}$–$F_I$ defects. All these components were assumed to have the same line broadening, isomer shifts that follow the second-order Doppler shift, and temperature-independent quadrupole splittings. D1c turned out to be too small to be constrained by the analysis. It was restricted to have twice the quadrupole splitting of D1a and the area ratio of D1c to D1b was restricted to be 1/7, assuming random distribution. The final analysis of the spectra is shown in Fig. 7 and the hyperfine parameters of the doublet components are given in Table II.

The isomer shift of D1a of $\delta_{RT} = 1.27(2)$ mm/s is not within the range of isomer shifts expected for low-spin $Fe^{2+}$ [1], which extends from −0.25 to 0.4 mm/s. However, applying the model of Nishihara and Ogawa [31], which takes into account nearest-neighbor distances and electronegativity in the range $\Delta\chi_P = 0.27$–$0.73$ of low-spin $Fe^{2+}$, isomer-shift value of $\delta_{RT} = 1.32$ mm/s is obtained, which is in excellent agreement with our observed value.

TABLE II. Hyperfine parameters of doublet components obtained from the analysis of the eMS spectra obtained of LiF (Fig. 7) and tentative site assignments.

| Component | $\delta_{RT}$ (mm/s) | $\Delta E_{Q,RT}$ (mm/s) | $\Delta\sigma$ (mm/s) | Tentative assignment |
|---|---|---|---|---|
| SL | 1.29(1) | | 0.02(1) [c] | $Fe_{Li}^{1+}$ (LS) |
| D1a | 1.27(2) | 1.12(3) | | $Fe_{Li}^{2+}$(LS) − $F_I$ |
| D1b | 1.10(2)[a] | 1.49(3) | | $Fe_{Li}^{2+}$(LS) − $2F_I$ |
| D1c | | 2.25[b] | | $F_I$ − $Fe_{Li}^{2+}$(LS) − $F_I$ |
| D2 | 0.59(3) | 3.2(7) | 0.08(3) | Unknown |

[a]Isomer shift of D1b and D1c set to be the same.
[b]Set to be double the quadrupole splitting of D1a.
[c]Same broadening assumed for all SL and D1 components.

The area fractions of the different components show no characteristic trend. The dominating feature is the *M* component, assigned to dilute high-spin paramagnetic $Fe^{3+}$ (likely stabilized by acceptor defects in amorphous zones created in the implantation process) which has ∼50% area fraction at 300 K, and ∼35% at $T > 400$ K. The area ratio of D2 increases from ∼0% at 300 K to ∼12% at 750 K. The area ratio of SL and the D1 components scatter between 10 and 20% throughout the temperature range. No definite signs of fluence dependence of the spectral areas were observed and no evidence for a component with a low Debye temperature suggesting pure interstitial Fe.

### C. Theory

To interpret the charge and spin state of Fe substituting for octahedrally coordinated $Na^+$/$Li^+$ in defect-free NaCl and LiF, respectively, the partial density of states (PDOS) of Fe around the Fermi energy and the total density of states (DOS) was calculated. Only $Fe^{1+}$ was observed without introduction of structural defects. Figure 8 show the total DOS and PDOS of Fe substituting the Na and Li site in NaCl and LiF, respectively. From the obtained charge state of Fe of 1+, the spin arrangement ($3t_{2g}\uparrow, 2e_g\uparrow, 2t_{2g}\downarrow$) and the total (orbital and spin) magnetic moment of the Fe atoms of 2.89 $\mu_B$ and 2.74 $\mu_B$ in NaCl and LiF, respectively, the results are consistent with high-spin, $S = 3/2$ state.

The high-spin configuration obtained is inconsistent with EPR results which suggested low-spin configuration and the calculated isomer shift differed significantly from the experimental values (see Table III). To obtain a low-spin configuration, one needed to (a) start the DFT calculations from a state of low spin [18] and (b) remove an electron from the total number of electrons (method applied in Ref. [32]) to account for the difference in the natural charge state of Fe from 2+ to 1+ when Fe replaces $Na^{1+}$ or $Li^{1+}$. In this way, results consistent with low-spin $Fe^{1+}$ were obtained.

Figure 9 show the total DOS and PDOS of Fe substituting the Na and Li site in NaCl and LiF, respectively, where the

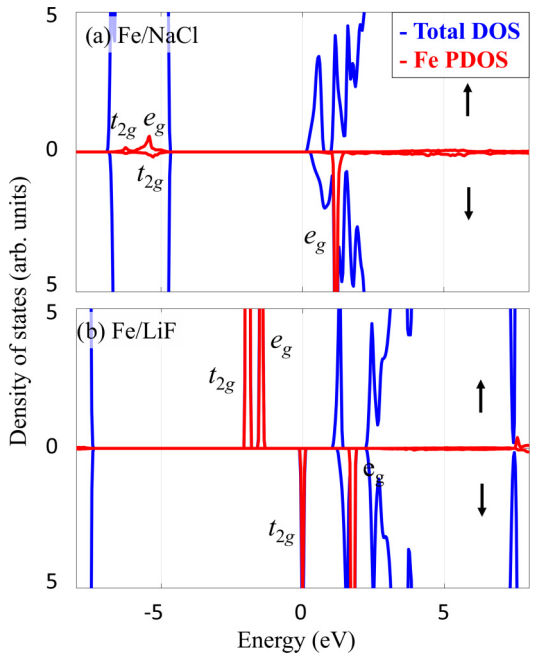


FIG. 8. Total density of states (DOS: blue color) and the partial density of states for $3d$ orbital (PDOS: red color) of (a) $Fe^{1+}$, $S = 3/2$ substituting the Na site at NaCl and (b) $Fe^{1+}$, $S = 3/2$ substituting the Li site at LiF.

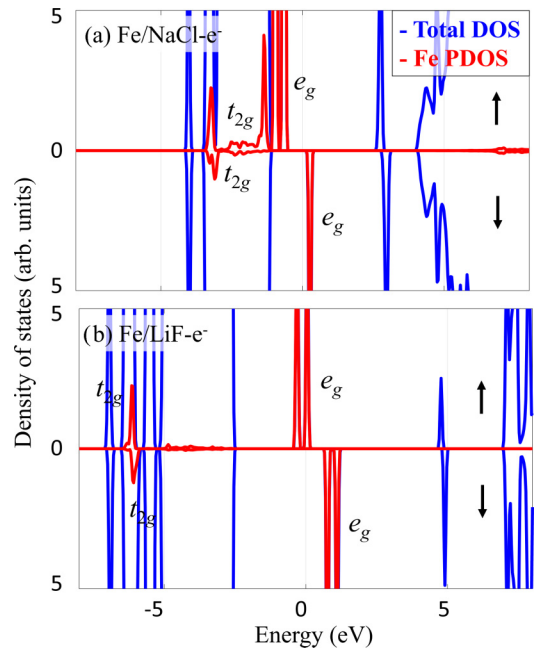


FIG. 9. Total DOS (blue color) and the PDOS (red color) for $3d$ orbital of (a) $Fe^{1+}$, $S = 1/2$ substituting the Na site and (b) $Fe^{1+}$, $S = 1/2$. substituting the Li site. DFT calculations were initiated from a low-spin state and with removing one electron, Fermi energy is defined at the energy of zero.

requirement of initiating calculations in low-spin state and removal of electron was applied. The spin arrangement of the $d$ band has changed to ($3t_{2g} \uparrow$, $1e_g \uparrow$, $3t_{2g} \downarrow$) and the total (orbital and spin) magnetic moment of the Fe atoms of 1.14 $\mu_B$ and 0.92 $\mu_B$ in NaCl and LiF, respectively, are consistent with low-spin, $S = 1/2$ state.

By removing an electron, the electronic valence charge around the Fe atoms has changed, leading to overlap for orbital of Fe ($3d$) and Cl, F ($3p$, $2p$) in the valence band, indicating that there is strong hybridization between orbitals in the case of low-spin state as evident in Fig. 9 in comparison with Fig. 8.

The stability of $Fe^{1+}$-doped NaCl was investigated by calculating the formation energy ($E_f$) in both low-spin and high-spin configuration by using the recipe in Ref. [33], taking into account the total energies of the defect and the pristine bulk (defect-free) structures, the chemical potentials calculated with the total energies of Na, Li, and Fe in the bulk body-centered cubic phase, charge state of the defect, and the energy at the valence-band maximum of the structure with defects.

The results from calculation are summarized in Table III. The values of isomer shift obtained for the low-spin state are in good agreement with the experimental values $\delta_{RT} = 1.19(2)$ mm/s in NaCl and $\delta_{RT} = 1.29(1)$ mm/s in LiF; the values for the high-spin state do not compare as well. The formation energies are significantly lower for the Fe impurity in NaCl and LiF structure in the low-spin case, demonstrating it to be the most energetically favorable configuration.

## IV. DISCUSSION

Of particular interest is whether the data for the low-spin $Fe^{1+}$ obtained in the present study are consistent with the variation of isomer shift as a function of the difference in electronegativity of the host atoms ($\Delta\chi_P$) proposed in the semiempirical model of Gunnlaugsson and Masenda [27] for high-spin $Fe^{2+}$ for a nearest-neighbor distance of $d_{nn} = 2$ Å ($\delta_{RT,\ 2\ Å}$). This requires knowledge of the dependence of isomer shift on nearest-neighbor distance ($d_{nn}$). Although there is too little information to establish this

TABLE III. Results from theoretical calculations on Fe defects in NaCl and LiF explained in the text. Table lists the spin, magnetic moment of Fe, calculated Mössbauer isomer shift ($\delta_C$), and formation energy ($E_f$). In all cases the quadrupole splitting of 0 mm/s was determined, as expected from the cubic symmetry.

| Configuration | Spin | Magnetic moment of Fe ($\mu_B$) | $\delta_C$ (mm/s) | $E_f$ (eV) |
|---|---|---|---|---|
| High-spin $Fe^{1+}$ on Na site in NaCl | 3/2 | 2.89 | 1.71 | 5.03 |
| Low-spin $Fe^{1+}$ on Na site in NaCl | 1/2 | 1.14 | 1.33 | 4.52 |
| High-spin $Fe^{1+}$ on Li site in LiF | 3/2 | 2.74 | 1.64 | 11.15 |
| Low-spin $Fe^{1+}$ on Li site in LiF | 1/2 | 0.92 | 1.21 | −0.08 |

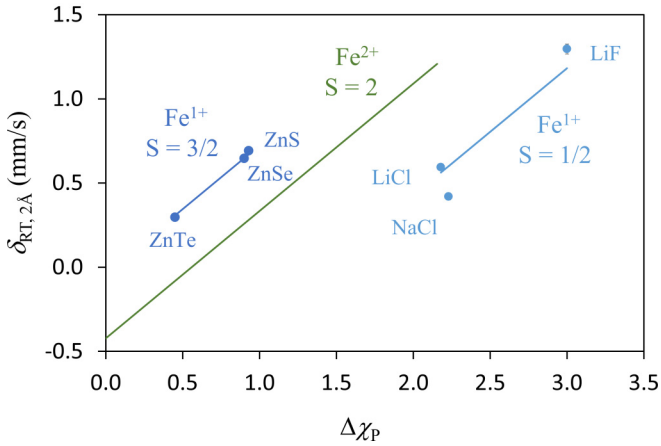


FIG. 10. Isomer shifts calculated for $d_{nn} = 2$ Å ($\delta_{RT,\,2Å}$) as a function of difference in electronegativity of the host atoms for the charge-/spin-state combinations indicated. Trend observed for high-spin $Fe^{2+}$ is from Ref. [27]. Data for $Fe^{1+}$, $S = 3/2$ obtained from metastable configuration (aftereffects) following decay of $^{57}$Co-doped samples [34–36]. For $Fe^{1+}$, $S = 1/2$, the data for LiCl are from Ref. [7] while data for LiF and NaCl are from this work.

relationship reliably, one can assume the same dependence as was found in Ref. [27] for high-spin $Fe^{2+}$, that is $\delta_{RT,\,2Å} = \delta_{RT} - 0.94(d_{nn} - 2$ Å$)$ mm/s. The data are shown in Fig. 10, with comparison with literature data on high-spin $Fe^{1+}$.

Although there are not enough data to firmly confirm the trend presented in Fig. 10, it is possible to conclude that the three charge-/spin-state configurations are distinguishable in a $\Delta\chi_P$–$\delta_{RT,\,2Å}$ plot which, thereby, further supports the identification of dilute Fe in NaCl and LiF as due to low-spin $Fe^{1+}$. The calculated values of isomer shifts of low-spin $Fe^{1+}$ state in NaCl and LiF (Table III) are close to the observed one and the calculated values for high-spin $Fe^{1+}$ are significantly higher, as expected from a trend extrapolating the data obtained from $^{57}$Co-doped samples [34–36].

Both $Cl^-$ and $F^-$ ligands are at the beginning of the spectrochemical series [37] and one could expect that $Fe^{1+}$ in both NaCl and LiF should be in high-spin configuration. The present results do not offer an explanation why this expectation is inconsistent with EPR data and the trends displayed in Fig. 10.

We observe, with eMS, $Fe^{1+}_{Na} - V_{Na}$ pairs in NaCl (D1 component) up to $T > 500$ K, although EPR literature suggests that these pairs are unstable above ∼200 K [11,12]. This implies that $Mn^{2+}_{Na} - V_{Na}$ pairs are stable during the half-life $T_{1/2} = 1.5$ min of $^{57}$Mn. The stability of such pairs has been well documented where the mobility of the pairs results in the formation of the Suzuki phase in NaCl after slow cooling from 400 °C to room temperature [38]. Following the $\beta^-$ decay of $^{57}$Mn in $Mn^{2+}_{Na} - V_{Na}$ pairs, the daughter $^{57*}Fe^{+}$ is "born" with a nearby Na vacancy. A single "jump" of the sodium vacancy within the measurement time is required to transform the $Fe^{1+}_{Na} - V_{Na}$ pair to a $Fe^{1+}_{Na}$ center. This takes place at ∼200 K for an annealing time of 2 min [12], and at ∼350 K during the 140-ns lifetime of $^{57*}$Fe (using the temperature where the area ratio of SL and D1 change the most in Fig. 4). Taking into account the different temperatures and timescales of the two experiments, the activation energy of vacancy jump can be estimated to be within the range 0.6–0.9 eV, which is in good agreement with the value 0.72 eV from Ref. [11]. This further supports the identification of D1 as due to $Fe^{1+}_{Na} - V_{Na}$ pairs and the identification of SL as due to $Fe^{1+}_{Na}$.

It is proposed here that the D1 components (D1a,b,c) in LiF are due to low-spin $Fe^{2+}$ coupled to $F^-$ interstitials [$Fe^{2+}_{Li}$(LS) $- nF_I$, $n = 1, 2$]. This is based on the charge compensation and the negligible temperature dependence of the quadrupole splitting, which suggest an $S = 0$ state. The isomer shift is found to be consistent with the empirical model of Nishihara and Ogawa [31] for low-spin $Fe^{2+}$ compounds, supporting this conclusion. Additional supporting evidence is that the addition of a second interstitial fluorine neighbor (D1b and D1c components) in the vicinity of the Fe probe, should result in shorter nearest-neighbor distances, and according to the model of Nishihara and Ogawa [31] result in a lowering of the isomer shift, which is what is observed (Table II).

$Mn^{2+}_{Li}$(LS) $- nF_I$ pairs would be formed during the lifetime of the $^{57}$Mn ($T_{1/2} = 1.45$ min.) and observed ∼100 ns after the $\beta^-$ decay with the $^{57}$Fe daughter. Therefore, it is relevant to compare our results with findings from EPR and photoluminescence studies of Mn-doped LiF.

Böttcher *et al.* [39] and Gago Bousquet *et al.* [40] found two distinct EPR spectra of $Mn^{2+}$-doped LiF, an orthorhombic spectrum and an axial spectrum of low intensity. The orthorhombic spectrum was assigned to a negatively charged chemical impurity and Li vacancy and the weak spectrum suggested association with two negatively charged chemical impurities [40]. Rearrangement of the $F^-$ ligands was required in the explanations of the EPR spectra.

The chemical impurity was not identified, but the results were consistent with the interpretation of that the chemical impurity is $OH^-$ group replacing $F^-$ [41,42]. It is unlikely that in random implantation measurements (and at the low total fluences employed here), that the Mn atoms come to rest beside an $OH^-$ neighbor. However, the orthorhombic nature of the site is consistent with crystal-field splitting needed to explain the $S = 0$.

Moreno *et al.* [43] reported double-excitation peaks in photoluminescence data related to the formation of precipitated phases containing $Mn^{2+}$ in the alkali halide lattice. For LiF:$Mn^{2+}$ the data suggested an anomalously small $Mn^{2+}$-F distance. Such shortening of the bonds would be expected for interstitial type of defect.

It cannot be stated with confidence at this stage whether the D1 components have any association with the centers observed by EPR or photoluminescence. Charge compensation with Li vacancies alone would be expected to give too small quadrupole interaction, therefore leaving interstitial $F^-$ as the obvious alternative explanation/interpretation.

It is generally assumed that iron cannot adopt the 1+ state in simple crystals. $Fe^{1+}$ has been observed by Mössbauer spectroscopy in complexes in organometallic and biochemical compounds (see, e.g., the discussion in Chap. 8 of Ref. [44]) and as metastable states in $^{57}$Co-doped samples [34–36]. The data presented here and the interpretation of the isomer shift of Fe in in LiCl and NaCl [7,8], demonstrate that $Fe^{1+}$ is a stable configuration in NaCl and LiF.

Clearly, it should be possible to promote high-spin $Fe^{1+}$ as a dilute Fe dopant in compounds with alkali metals from elements from chalcogens and/or halogens groups where their local coordination is tetrahedral. This could be dilute Fe in, for example, $Na_2O$ and similar compounds with antifluoride structure. Similarly, the low-spin state can be promoted in sufficiently strong octahedral ligand fields, potentially other rocksalt compounds. $^{57}$Fe emission Mössbauer spectroscopy using implantation of $^{57}$Mn appears to be a promising technique to obtain data on these systems, giving simultaneous information about the dilute substitutions of Fe and on Mn-related defects.

## V. CONCLUSIONS

There is overwhelming evidence that dilute-substitutional Fe in NaCl and LiF is in a low-spin $Fe^{1+}$ configuration. This interpretation is in accordance with EPR results and the isomer shift observed in Mössbauer studies of Fe-implanted samples when ligand distances and the difference in electronegativity of the host atoms are taken into account and supported by DFT calculations of isomer shifts and formation energies in these systems.

Metastable low-spin $Fe^{1+}$ coupled to Na vacancy is observed in NaCl, owing to the formation of $Mn^{2+}_{Na} - V_{Na}$ during the lifetime ($T_{1/2} = 1.45$ min.) of the $^{57}$Mn parent. Similar coupling of $Mn^{2+}$ to lithium vacancy in LiF is not observed; instead, low-spin $Fe^{2+}$ coupled to $F^-$ interstitials is observed. This suggests that while the Na vacancy is the dominant charge-compensating defect in NaCl, interstitial $F^-$ is the dominating charge-compensating defect in LiF. The results present an interpretation on the nature (i.e., charge and spin states) of Fe dopants in metal halides and prompt for further experimental and theoretical studies on related materials systems.

## ACKNOWLEDGMENTS

We acknowledge the support of the ISOLDE Collaboration and technical teams and cluster resources provided by CERN (HTC/Condor). G. Marschick (Vienna University of Technology, Austria; University Duisburg-Essen, Germany & CERN, Switzerland) is acknowledged for experimental help. B. Qi (University of Iceland, Iceland) is acknowledged for fruitful discussions. S.O. acknowledges support from the University of Iceland Research Fund. R.A. acknowledges the funding of the Austrian Science Fund (FWF) through Projects No. P26830 and No. P31423. The Federal Ministry of Education and Research (BMBF) through Grants No. 05K16PGA and No. 05K19SI1 "eMMA" is acknowledged. The European Commission through the Horizon 2020 programme (Grant No. 654002, ENSAR 2) is acknowledged. K.B.-R., H.M., D.N., K.N., and G.P. acknowledge support of the Department of Science & Innovation (South Africa) within the SA-CERN Program. I.U. acknowledges the support of the Ministry of Economy and Competitiveness (MINECO/FEDER) under Project No. RTI2018-094683-B-C55 and Basque Government Grant No. IT-1500-22.

[1] N. N. Greenwood and T. C. Gibb, in *Mössbauer Spectroscopy* (Springer, Dordrecht, 1971).

[2] J. G. Mullen, Study of iron ions in NaCl using the Mössbauer Effect. II. The vacancy-impurity associated state, Phys. Rev. **131**, 1415 (1963).

[3] K. Henning and K. Yung, Mössbauer effect study of iron impurity states in AgCl and NaCl, Phys. Status Solidi **40**, 365 (1970).

[4] A. N. Murrin and P. P. Serein, Investigation of cobalt-, iron-, and tin-doped silver and alkali halides by the Mössbauer method, Phys. Status Solidi A **2**, 663 (1970).

[5] S. M. Edelglass and M. Ohring, Deformation-induced Mössbauer spectra in NaCl, Phys. Status Solidi A **17**, 567 (1973).

[6] A. G. Maddock, A. F. Williams, K. E. Siekierski, and J. Finger, The Mössbauer emission spectra of impurity $^{57}$Cobalt in a halide matrix, Phys. Status Solidi B **74**, 183 (1976).

[7] N. Kai, Mössbauer spectroscopic study of alkali chloride crystals containing a small amount of iron (II), J. Shimonoseki Univ. Fish. **30**, 63 (1981).

[8] D. Barb, S. Constantinescu, S. Nistor, and D. Tarina, Mössbauer spectroscopy on $^{57}$Fe:NaCl crystals, Hyperfine Interact. **53**, 279 (1990).

[9] K. Suzuki, X-ray studies on precipitation of metastable centers in mixed crystals NaCl-$CdCl_2$, J. Phys. Soc. Jpn. **16**, 67 (1961).

[10] R. Mantovan, H. P. Gunnlaugsson, K. Johnston, H. Masenda, T. E. Mølholt, D. Naidoo, M. Ncube, S. Shayestehaminzadeh, K. Bharuth-Ram, M. Fanciulli, H. P. Gislason, G. Langouche, S. Ólafsson, L. M. C. Pereira, U. Wahl, P. Torelli, and G. Weyer, Atomic-scale magnetic properties of truly 3d-diluted ZnO, Adv. Electron. Mater. **1**, 1400039 (2015).

[11] B. R. Yang, A. Bouwen, and D. Schoemaker, Electron spin resonance study of $Fe^+$ centers in NaCl : $Fe^{++}$ and motion of the associated vacancies, Phys. Status Solidi B **127**, 657 (1985).

[12] S. V. Nistor, M. Velter Stefanescu, and D. C. Mateescu, A study on $Fe^+$ centers in NaCl crystals, Solid State Commun. **53**, 989 (1985).

[13] T. P. P. Hall, W. Hayes, R. W. H. Stevenson, and J. Wilkens, Investigation of the bonding of iron-group ions in fluoride crystals, II, J. Chem. Phys. **39**, 35 (1963).

[14] H. R. Anand, Mössbauer study of dispersed iron ions in alkali halides, Phys. Status Solidi B **84**, 227 (1977).

[15] V. N. Fedoseyev, K. Bätzner, R. Catherall, A. H. M. Evens, D. Forkel-Wirth, O. C. Jonsson, E. Kugler, J. Lettry, V. I. Mishin, H. L. Ravn, and G. Weyer, and the ISOLDE Collaboration, Nucl. Instrum. Methods B **126**, 88 (1997).

[16] G. Weyer, in *Mössbauer Effect Methodology*, edited by I. J. Gruverman and C. W. Seidel (Plenum, New York, 1976), Vol. 10, p. 301.

[17] H. P. Gunnlaugsson, Spreadsheet based analysis of Mössbauer spectra, Hyperfine Interact. **237**, 79 (2016).

[18] P. Blaha, K. Schwarz, G. K. Madsen, D. Kvasnicka, and J. Luitz, *An Augmented Plane Wave + Local Orbital Program for Calculating Crystal Properties* (Techn. Universitat Wien, Austria, 2001); see http://www.wien2k.at/.

[19] P. Blaha, K. Schwarz, F. Tran, R. Laskowski, G. K. Madsen, and L. D. Marks, WIEN2k: An APW+lo program for calculating the properties of solids, J. Chem. Phys. **152**, 074101 (2020).

[20] J. P. Perdew, K. Burke, and M. Ernzerhof, Generalized Gradient Approximation Made Simple, Phys. Rev. Lett. **77**, 3865 (1996).

[21] K. Wang and R. R. Reeber, Thermal expansion of alkali halides at high pressure: NaCl as an example, Phys. Chem. Miner. **23**, 354 (1996).

[22] R. W. G. Wyckoff, *Crystal Structures 1*, 2nd ed. (Interscience, New York, 1963).

[23] F. Neese, Prediction and interpretation of the $^{57}$Fe isomer shift in Mössbauer spectra by density functional theory, Inorg. Chim. Acta **337**, 181 (2002).

[24] U. D. Wdowik and K. Ruebenbauer, Calibration of the isomer shift for the 14.4 keV transition in $^{57}$Fe using the full-potential linearized augmented plane-wave method, Phys. Rev. B **76**, 155118 (2007).

[25] P. Dufek, P. Blaha, and K. Schwarz, Determination of the Nuclear Quadrupole Moment of $^{57}$Fe, Phys. Rev. Lett. **75**, 3545 (1995).

[26] W. J. L. Buyers and T. Smith, The Debye-Waller factors of sodium chloride, J. Phys. Chem. Solids **25**, 483 (1964).

[27] H. P. Gunnlaugsson and H. Masenda, Mössbauer isomer-shift of ferrous iron impurities in ionic and covalent binary compounds, J. Phys. Chem. Solids **129**, 151 (2019),.

[28] V. C. Nelson and R. J. Friauf, Diffusion of vacancies and vacancy pairs in NaCl, J. Phys. Chem. Solids **31**, 825 (1970).

[29] T. E. Mølholt, R. Mantovan, H. P. Gunnlaugsson, D. Naidoo, S. Ólafsson, K. Bharuth-Ram, M. Fanciulli, K. Johnston, Y. Kobayashi, G. Langouche, H. Masenda, R. Sielemann, G. Weyer, and H. P. Gíslason, Observation of spin-lattice relaxations of dilute $Fe^{3+}$ in MgO by Mössbauer spectroscopy, Hyperfine Interact. **197**, 89 (2010).

[30] T. E. Mølholt, H. P. Gunnlaugsson, K. Johnston, R. Mantovan, H. Masenda, S. Ólafsson, K. Bharuth-Ram, H. P. Gislason, G. Langouche, and G. Weyer, and The ISOLDE Collaboration, Spin-lattice relaxations of paramagnetic $Fe^{3+}$ in ZnO, Phys. Scr. **T148**, 014006 (2012).

[31] Y. Nishihara and S. Ogawa, Mössbauer study of $^{57}$Fe in the pyrite-type dichalcogenides, J. Chem. Phys. **71**, 3796 (1979).

[32] M. B. Barbosa, J. G. Correia, K. Lorenz, R. Vianden, and J. P. Araújo, Studying electronic properties in GaN without electrical contacts using $\gamma$-$\gamma$ vs $e^-$-$\gamma$ perturbed angular correlations, Sci. Rep. **9**, 15734 (2019).

[33] C. L. Yao, J. C. Li, W. Gao, A. Tkatchenko, and Qing Jiang, Effective scheme to determine accurate defect formation energies and charge transition levels of point defects in semiconductors, Phys. Rev. B **96**, 245203 (2017).

[34] T. Becze-Deák, L. Bottyán, P. Bonville, D. L. Nagy, B. Molnár, U. W. Pohl, and H. Spiering, Comparative Mössbauer spectroscopic study of iron impurities in ZnSe, J. Phys. Chem. Sol. **62**, 987 (2001).

[35] C. Garcin, P. Imbert, G. Jéhanno, A. Gérard, and J. Danon, $Fe^{1+}$ transient charge state in ZnS: $^{57}$Co Mössbauer sources, J. Phys. Chem. Solids **41**, 969 (1980).

[36] A. Gérard, C. Garcin, and P. Imbert, Observation by $^{57}$Fe Mossbauer spectroscopy of iron as electron traps and of the relaxation of these transient states in ZnTe and ZnS, J. Cryst. Growth **101**, 493 (1990).

[37] R. Tsuchida, Absorption spectra of co-ordination compounds. I, Bull. Chem. Soc. Jpn. **13**, 388 (1938).

[38] J. A. Chapman and E. Lilley, The structure of precipitates in Mn-doped NaCl, J. Mater. Sci. **10**, 1154 (1975).

[39] R. Böttcher, W. Windsch, and W. Lüdke, EPR investigation on $Mn^{2+}$-doped LiF single crystals, Phys. Status Solidi **20**, 121 (1967).

[40] C. Gago Bousquet, A. Serra Valls, and M. Garcia Sucre, EPR in LiF:$Mn^{2+}$ at 35 GHz, J. Magn. Reson. **6**, 117 (1972).

[41] G. D. Watkins, Electron spin resonance of $Mn^{++}$ in alkali chlorides: Association with vacancies and impurities, Phys. Rev. **113**, 79 (1959).

[42] A. Bianchini, M. Marinelli, S. Santucci, P. Berge, and C. Laj, $OH^-$ divalent cation complexes in NaF, Phys. Lett. A **29**, 522 (1969).

[43] M. Moreno, F. Rodríguez, J. A. Aramburu, F. Jaque, and F. J. López, Double excitation transitions in $Mn^{2+}$-doped alkali halides, Phys. Rev. B **28**, 6100 (1983).

[44] P. Gütlich, E. Bill, and A. X. Trautwein, *Mössbauer Spectroscopy and Transition Metal Chemistry* (Springer, Berlin, 2011).